



Simulating future land use/land cover of Tigris river basin assuming the continuation of the conditions during 2018 and 2023

Abolfazl Ghanbari^{1*}, Ayat Khaleel-Gharibawi¹, Hala Abdulkareem-Rubaiee¹,
Mehrdad Jeihouni¹

¹ Department of Remote Sensing and GIS, Faculty of Planning and Environmental Sciences, University of Tabriz, Tabriz, Iran. E-mail: a_ghanbari@tabrizu.ac.ir

Article Info.

ABSTRACT

Article type:

Research Article

Article history:

Received: 29 Oct. 2024

Received in revised from: 26 Nov. 2024

Accepted: 18 Dec. 2024

Published online: 27 Dec. 2024

Keywords:

Remote sensing,
Tigris River Basin,
Random forest,
Support vector machine,
CA-Markov,
LULC simulation.

Environmental planning and resource management necessitate an analysis of changes in land use and land cover (LULC). In recent years, climate change and human activities, notably the erection of the Ilisu dam, have adversely impacted the Tigris River Basin (TRB), one of the most vital natural resources in Western Asia, resulting in significant alterations in its LULC. Based on this, the present study developed multi-temporal (2003-2023) LULC maps for TRB through classifying Landsat images using the random forest (RF) and support vector machine (SVM) algorithms, and simulating future LULC states (2028) employing the cellular automata (CA)-Markov model. RF exhibited better performance than SVM in the classification of Landsat images, and its results were chosen for further investigation. The CA-Markov model simulated the landscape map of 2028 by considering LULC dynamics between 2018 and 2023. The model's performance was validated, confirming acceptable results with an accuracy rate of 0.798 and F1 score of 0.789. Notably, LULC changes in TRB were critical, including a reduction in water resources, wetlands and croplands. This could lead to several environmental challenges, highlighting the significance of quick LULC changes. The construction of the Ilisu Dam on the Tigris River in Turkey has worsened the situation by exacerbating water shortages, expanding bare ground, harming wetlands, reducing water quality, soil salinization, and damaging the aquatic ecosystems. The drying wetlands and expanding bare grounds will become potential dust sources in the future and affect surrounding countries. Accordingly, intergovernmental actions and special policies are needed to manage this environmental crisis.

Cite this article: Ghanbari, A., Khaleel-Gharibawi, A., Abdulkareem-Rubaiee, H., Jeihouni, M. (2024). Simulating future land use/land cover of Tigris river basin assuming the continuation of the conditions during 2018 and 2023. *DESERT*, 29 (2), DOI: 10.22059/jdesert.2024.100667



1. Introduction

Land use/land cover (LULC) changes have significant impacts on human life. Information on LULC proves necessary in various environmental applications, including managing hydrological processes, natural disasters, watersheds, and climate changes (Al-Taei *et al.*, 2023). While changes in LULC are a regular occurrence in the environment, the rapid LULC modifications resulting from economic and industrial development, as well as population growth, lead to detrimental environmental effects (Talukdar *et al.*, 2020). In recent times, human-induced changes in LULC have considerably influenced water quality and quantity, soil and air quality, soil erosion, biodiversity, and local to regional weather and climate conditions (Roy *et al.*, 2022).

The Tigris River basin (TRB), located in West Asia, has suffered significant damage due to human-induced LULC change in recent years (Brown *et al.*, 2022; Giovanis and Ozdamar, 2021). Since river basins are key elements in the environment and society, providing fresh water, controlling water quality and flow, safeguarding against natural hazards, and overseeing biodiversity conservation (Al-Taei *et al.*, 2023), LULC change in these areas could inflict considerable harm on the environment. The water crisis is a critical issue in this basin that requires further examination. While it is challenging to differentiate the impacts of natural and anthropogenic factors on water resources (Zucca *et al.*, 2021), inadequate water resource management plans and the absence of cooperation among riparian countries represent the two principal causes of the water crisis in TRB (Al-Madhhachi *et al.*, 2020).

One major concern regarding water scarcity in the TRB is the construction of the Ilisu dam, in Turkey, which has resulted in the destruction of numerous villages and displacement of countless people (Abatzoglou *et al.*, 2018). Moreover, the dam's construction has ecological implications for the Tigris Valley, and it affects water supply in the downstream areas of the basin, leading to a reduction in the water flow of the Tigris River. As a consequence, this results in heightened agricultural demands and disruption of natural habitats, as well as desertification and salinity in remote regions, and ultimately exacerbating water scarcity (Abatzoglou *et al.*, 2018).

In any river basin, water flow change can lead to significant LULC change. Therefore, it is crucial to study the LULC of TRB after the construction of the Ilisu dam. Remote sensing (RS) imagery has been used as a beneficial method for quantitatively investigating LULC change (Talukdar *et al.*, 2020). Satellite remote sensing provides practical means to collect information about LULC and detect its changes due to access to data at different temporal and spatial scales (Faruque *et al.*, 2022). Nonetheless, RS-based LULC change detection remains complex, particularly when the study area is extensive and morphological features are diverse, as conventional methods do not suffice to create LULC maps (Al-Taei *et al.*, 2023). Additionally, the varying spatial and temporal distribution of landscapes, as well as their distinct spectral characteristics, contribute to the complexity of LULC mapping (Aryal *et al.*, 2023; Momeni *et al.*, 2016). Machine learning can address these challenges as it can analyze hidden patterns and extract relevant information from the complex interdependencies between dependent and independent variables (Khorrami *et al.*, 2022).

Machine learning is a computational technique that allows computers to learn from data and make decisions or predictions without requiring explicit programming (El Naqa and Murphy, 2015). Additionally, machine learning algorithms possess immense potential for combining new exploratory variables to develop a data model for LULC mapping (Wang *et al.*, 2022). With the development of machine learning, improved access to remote sensing data, and enhanced computing power, generating LULC maps has become increasingly feasible. Various

machine learning algorithms have been effectively utilized in mapping LULC based on RS data, including classification and regression trees (Loukika *et al.*, 2021), random forest (RF) (Pan *et al.*, 2022), support vector machine (SVM) (Loukika *et al.*, 2021), artificial neural network (Ghayour *et al.*, 2021), minimum distance (Ghayour *et al.*, 2021), maximum likelihood classification (Singh and Pandey, 2021b), random trees (Singh and Pandey, 2021b), derivative-free multi-layer perceptron (Jamali, 2020), complex tree (Jamali, 2020), deep neural network (Abdi, 2020), and extreme gradient boosting (Abdi, 2020).

In addition to the necessity of LULC mapping with machine learning algorithms, it is also critical to simulate future LULC dynamics to clarify potential changes and consider measures to prevent potential risks (Beroho *et al.*, 2023). The frequently used model for LULC prediction is the Cellular Automata (CA)-Markov model. This open-structured spatial model improves LULC simulation functionality by operating on the transition probability of LULC classes (Beroho *et al.*, 2023). The CA-Markov model has been utilized in multiple studies to simulate forthcoming LULC scenarios that encompass predicting spatial and decadal LULC transformations (El Haj *et al.*, 2023), monitoring and projection of LULC (Abatzoglou *et al.*, 2018), and evaluating potential landscape risk (Atef *et al.*, 2023).

Although the TRB situation has considerable impacts on the environment and people's lives, to our knowledge, few studies have tackled the analysis of LULC changes in this region. Considering the above, this study aimed to simulate the future LULC scenario, focusing on the impact of the Ilisu dam on the TRB. To achieve this, Landsat satellite images from 2003 to 2023 were classified using RF and SVM as machine learning algorithms. Then, the CA-Markov model was employed to simulate the 2028 LULC map. The results will assist policymakers in identifying vulnerable regions and implementing suitable mitigation measures.

2. Materials and Methods

2.1. Study area

The Tigris River is among the largest rivers in the Middle East. Its basin, TRB, is shared by four nations: Iran, Iraq, Syria, and Turkey. The TRB has an estimated area of 279,000 square kilometers and is situated between the latitudes 30°59′ to 39° 19′ N and longitude 39°15′ to 48°34′ E. Water quantity, quality, and biodiversity are key concerns of this area. Climate projections for TRB indicate a decrease in precipitation and river flow, as well as an increase in temperature. Figure 1 shows the location map of the TRB.

2.2. Spatial database

In this study, three datasets of Landsat 7, surface reflectance (SR) Tier 1 (2003, 2008), Landsat 8 SR Tier 1 (2013, 2018, 2023), and the NASA digital elevation model (DEM) (2000) used in this study with spatial resolution of 30 m. They were obtained from the Google Earth Engine (GEE) (data accessed by the U.S. Geological Survey). To train supervised classification methods, sufficient and efficient samples are required. For LULC classification, each sample must have a LULC class label and a set of features. To create train samples, 50,000 random points were selected in the study area. These points were labeled by visual inspection in seven classes: water, trees, wetlands, croplands, built-up lands, barren, and rangeland. Sample points were distributed across the study area. This study selected several classification features based on the literature (Loukika *et al.*, 2021; Mishra *et al.*, 2019; Pan *et al.*, 2021; Singh and Pandey, 2021a; Tassi *et al.*, 2021; Yeneneh *et al.*, 2022; Zhong *et al.*, 2021) including morphological features, spectral bands, spectral indices, and textural features. In cases where there are variations in morphology, employing morphological characteristics is crucial for carrying out

LULC classification (Tassi *et al.*, 2021). Therefore, we extracted four features, namely: elevation, aspect, hill-shade, and slope, from the NASA-DEM. Additionally, we used nine other features derived from Landsat satellite imagery. These comprised six spectral bands including Red (R), Green (G), Blue (B), near-infrared (NIR), shortwave infrared (SWIR) 1, and SWIR 2, in addition to four spectral indices. Furthermore, the GLCM method generated 18 textural features. For more information regarding these GLCM texture features, refer to (Mohanaiah *et al.*, 2013).

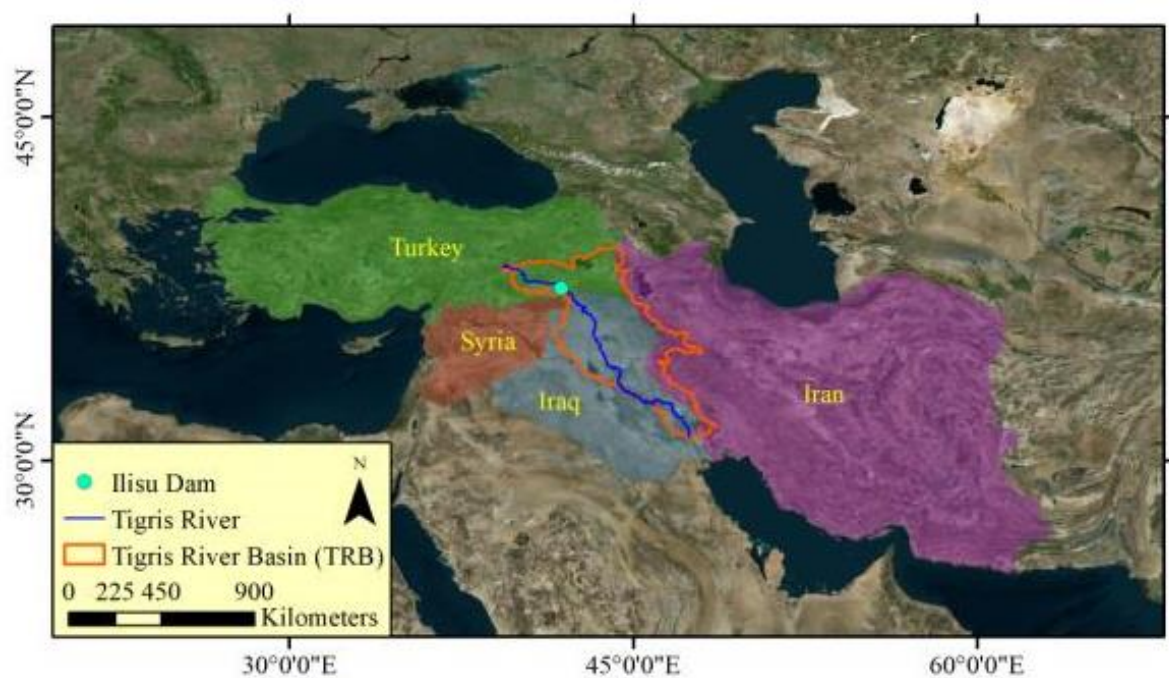


Figure 1. Location map of the study area

Spectral indices enhance LULC classification by providing more information (Capolupo *et al.*, 2020; Singh *et al.*, 2016), where each spectral index detects a specific LULC class. This study employed bare soil index (BSI), modified normalized difference water index (MNDWI), normalized difference built-up index (NDBI), and normalized difference vegetation index (NDVI) for improved classification precision. BSI is practical for discriminating bare soil and other LULC classes and improves the detection of bare soil areas (Chen *et al.*, 2004; Diek *et al.*, 2017). Classifying built areas is challenging as they are similar to bare soil areas in spectral characteristics. NDBI is a beneficial index for mapping built areas. NDVI is a standard vegetation index that directly measures vegetation health (Tassi *et al.*, 2021). Built areas are correlated with water bodies in some indices. MNDWI is used to overcome this issue and for better discrimination of water features (Xu, 2006). The spatial distribution of tonal variations in an image creates a visual effect called texture. Texture analysis is a standard method that uses the spatial features of an image to obtain valuable new information for its interpretation. Accordingly, textural features are helpful for accurate LULC classification (Mishra *et al.*, 2019).

2.3. Methods

2.3.1 Land use/Land cover (LULC) classification

According to the literature (Abdi, 2020; Al-Taei *et al.*, 2023; Ghayour *et al.*, 2021; Jamali, 2020; Loukika *et al.*, 2021; Pan *et al.*, 2021; Roy, 2021; Singh and Pandey, 2021a; Talukdar *et al.*, 2020; Yeneneh *et al.*, 2022; Zhong *et al.*, 2021), both SVM and RF classifiers have demonstrated high accuracy in LULC classification. Therefore, these classifiers were utilized in the current study RF utilizes both decision tree and ensemble learning concurrently, resulting in increased interpretability and accuracy. Additionally, RF generates a large number of trees with minimal overfitting. SVM is a frequently employed machine learning algorithm with exceptional generalization abilities and high modeling precision. Moreover, SVM optimization and input space are independent of one another (Farhangi *et al.*, 2023).

2.3.1.1. Random forest (RF) algorithm

RF is an ensemble learning algorithm utilizing a group of decision trees for modeling. Even minor changes in a decision tree's structure can result in significant performance improvements. Decision trees are practical, fast, and simple algorithms that are susceptible to overfitting. Therefore, RF generates numerous decision trees randomly to mitigate the overfitting issue while maintaining the simplicity, speed, and practicality of decision trees. RF modeling starts by randomly dividing the data into a training group (the in-bag) and a validation group (the out-of-bag). Then, multiple decision trees are created using bootstrap sampling from the dataset. In regression problems, the final prediction is obtained by averaging predictions from all trees. In classification problems, the final prediction is achieved by voting between all trees (Khorrami *et al.*, 2022). Reducing the correlation among trees, enhancing the performance of each tree, and considering computational constraints are three primary factors that affect RF performance (Farhangi *et al.*, 2021).

2.3.1.2. Support vector machine (SVM) algorithm

SVM is a robust supervised machine learning method that effectively addresses regression and classification problems. SVMs have the ability to handle high-dimensional data and nonlinear relationships. Given n features, the SVM constructs an n -dimensional space, mapping samples onto it with the aid of a kernel function (Farhangi, 2022). The transformed samples are then separated by a hyperplane. The objective is to maximize the margin between the closest samples of different classes using the best hyperplane, which minimizes the classification error. In addition, SVMs are extensively employed in various fields and they can perform well even with limited training data (Farhangi *et al.*, 2022).

2.3.2. Land use/land cover (LULC) simulation

2.3.2.1. Markov model

Markov is an effective model for predicting trends in LULC changes. It calculates the probability of transition from one state to another by using a transition probability matrix. However, the Markov chain only accounts for the transition probability within two-time steps, without considering the impact of neighboring cells on LULC predictions (Siddiqui *et al.*, 2018).

The Markov model performs the prediction as follows (Mondal *et al.*, 2016):

$$S(t + 1) = P_{i,j} \times S(t) \quad (1)$$

where $S(t+1)$ and $S(t)$ are the LULC status at the time of t and $t+1$, respectively. $P_{i,j}$ is the

transition probability matrix calculated by Eq. 2 (Mondal *et al.*, 2016).

$$P_{i,j} = \begin{bmatrix} P_{1,1} & P_{1,2} & \cdots & P_{1,n} \\ P_{2,1} & P_{2,2} & \cdots & P_{2,n} \\ \cdots & \cdots & \cdots & \cdots \\ P_{n,1} & P_{n,2} & \cdots & P_{n,n} \end{bmatrix}, \quad \sum_{j=1}^n P_{i,j} = 1 \quad (2)$$

2.3.2.2. Cellular automata (CA)-Markov model

CA is a prominent spatial modeling technique for examining proximity, a crucial spatial element showcasing LULC change dynamics. CA posits that an area has a greater propensity to change to a LULC class if its adjoining areas belong to that class. This technique partitions the study area into a grid of cells, with each cell denoting a section of the study area. It subsequently computes the subsequent state of each cell founded on its four primary components: cellular space and cell, neighboring cells, cell state, and transition rules (Gharaibeh *et al.*, 2020):

$$S(t, t + 1) = f(S(t), N) \quad (3)$$

where S is a set of discrete and limited cell states, N is the neighboring cells, t illustrates time, and f is the transition rule of cell states in the local space.

The CA-Markov model is introduced by applying derived transition rules from the Markov model. This model is regularly utilized for simulating LULC, and considers both spatial and temporal changes. The CA-Markov model utilizes a combination of the CA filter and Markov chain procedure to predict changes in LULC over time (Kang *et al.*, 2019).

2.3.3. Classification validation

In this study, accuracy and F1 score were selected to validate the performance of the RF model. Accuracy generally depicts the classifier's performance across all LULC classes, making it useful when all classes have equal importance (Basheer *et al.*, 2022). The F1 score represents the harmonic mean of precision and recall, considering both measures simultaneously. Precision indicates the proportion of the samples that are correctly classified within the samples predicted positive, and recall represents the proportion of correct classifieds in all really true samples (Francini *et al.*, 2022). Both accuracy and F1 score are computed using true positive (TP), true negative (TN), false positive (FP), and false negative (FN) values. TP represents the positive samples predicted as positive, TN is the number of negative samples predicted as negative, FP is negative samples predicted as positive, and FN is positive samples predicted as negative. Accuracy and F1 score are computed as follows (Al-Taei *et al.*, 2023):

$$Accuracy = \frac{TP+TN}{TP+TN+FP+FN} \quad (4)$$

$$F1 = \frac{2 \times Precision \times Recall}{Precision + Recall} = \frac{2 \times TP}{2 \times TP + FP + FN} \quad (5)$$

2.4. Methodology

The research procedure is shown in Figure 2. It includes seven main steps as follows:

1. Data preparation: Three data sets including Landsat 7 SR Tier 1, Landsat 8 SR Tier 1, and NASA-DEM (2000) were collected and processed.
2. Feature Extraction: Six spectral bands, four spectral indices, and 18 textural features were extracted from Landsat images. The gray-level co-occurrence matrix (GLCM)

method utilized for textural features. NASADEM digital elevation model was processed to calculate aspect, elevation, hill-shade, and slope.

3. Feature selection: To improve classification, the Gini index evaluated the features importance and 16 features with the lowest weights were removed.
4. Sample Labeling: Fifty-thousand sample points within the study area were randomly selected and visually inspected for labeling.
5. Classification LULC: 75% of the provided samples were utilized to train two RF and SVM, while the remaining 25% of samples were used for classifier validation.
6. Detection of LULC changes: Initially, we created multitemporal LULC maps using the RF, which proved most accurate. Subsequently, these maps were compared with each other to detect any significant changes in the LULC.
7. Simulation of LULC Change: The transition matrix of the Markov chain was computed initially, incorporating the LULC changes taking place between 2018 and 2023. Subsequently, a CA-Markov model applied to simulate the 2028 map.

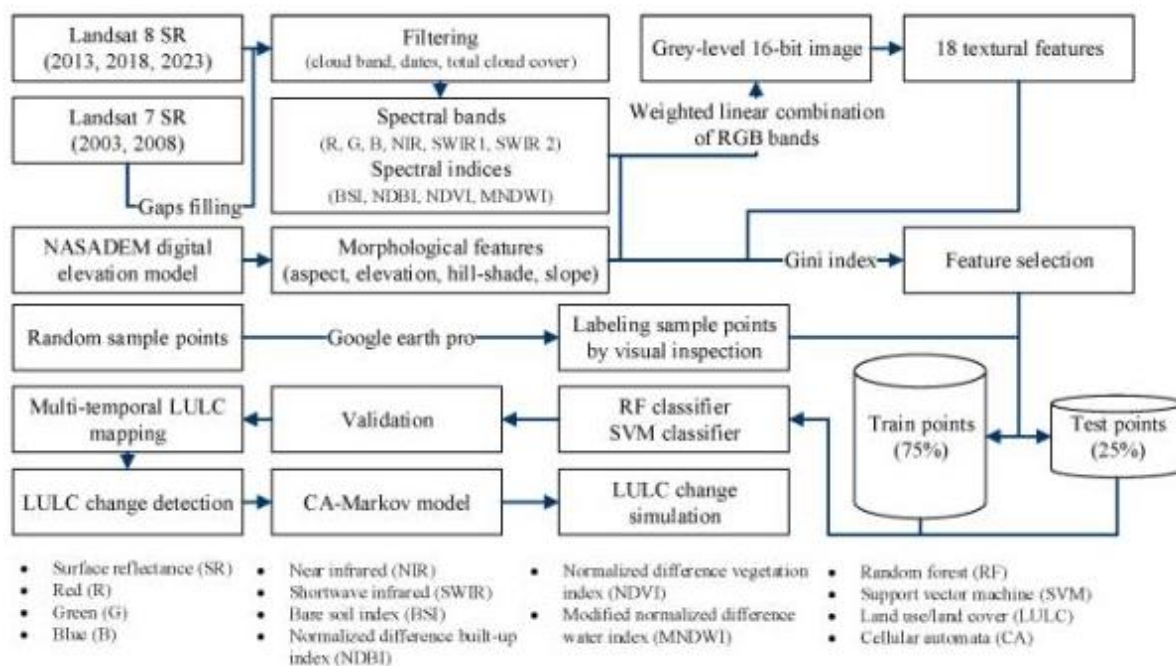


Figure 2. Research methodology

3. Results and Discussion

3.1. Land use/land cover (LULC) classification

RF and SVM maps were generated using Google Earth Engine. The classification process utilized 32 features derived from Landsat 7, Landsat 8, and NASADEM, with LULC classes serving as the dependent variable. Prior to training the classifiers, a thorough feature selection was performed using the Gini index. Table 1 presents the Gini index results, which ranked the features based on their importance. Subsequently, the top 50% of features with the highest importance weights were retained for classification, resulting in the exclusion of 16 less relevant features.

On average, the most significant variables influencing LULC classification were morphological features, spectral indices, spectral bands, and textural features. The high

importance of morphological features can be explained by the varied topography of TRB, which is partly mountainous (Issa *et al.*, 2014). The diverse geomorphology of the basin, characterized by mountainous regions and valleys, highlights the importance of elevation and slope in differentiating land cover types (Issa *et al.*, 2014). Spectral indices, such as NDVI and NDBI, also ranked highly due to their ability to enhance classification accuracy by emphasizing biophysical properties like vegetation health and urbanization (Al-Taei *et al.*, 2023). Lastly, The limited significance of textural features in this analysis can likely be attributed to the spatial resolution of the imagery, which may not adequately capture the fine-scale patterns required to differentiate certain land cover types (Feng *et al.*, 2015).

Table 1. Gini index outputs for feature selection

Feature	Feature type	Average importance weight	Status
Elevation	Morphological feature	0.049	Selected
MNDWI	Spectral index	0.044	Selected
Slope	Morphological feature	0.043	Selected
SWIR 2	Spectral band	0.041	Selected
NDVI	Spectral index	0.041	Selected
BSI	Spectral index	0.040	Selected
NDBI	Spectral index	0.040	Selected
SWIR 1	Spectral band	0.039	Selected
NIR	Spectral band	0.039	Selected
Texture_savg	Textural feature	0.039	Selected
G	Spectral band	0.038	Selected
R	Spectral band	0.038	Selected
B	Spectral band	0.038	Selected
Texture_shade	Textural feature	0.037	Selected
Texture_corr	Textural feature	0.037	Selected
Texture_dvar	Textural feature	0.036	Selected
Texture_idm	Textural feature	0.035	Removed
Aspect	Morphological feature	0.033	Removed
Texture_prom	Textural feature	0.033	Removed
Texture_diss	Textural feature	0.033	Removed
Texture_svar	Textural feature	0.033	Removed
Texture_contrast	Textural feature	0.033	Removed
Texture_inertia	Textural feature	0.033	Removed
Texture_var	Textural feature	0.032	Removed
Hill shade	Morphological feature	0.026	Removed
Texture_imcorr1	Textural feature	0.020	Removed
Texture_dent	Textural feature	0.011	Removed
Texture_ent	Textural feature	0.011	Removed
Texture_imcorr2	Textural feature	0.010	Removed
Texture_asm	Textural feature	0.010	Removed
Texture_sent	Textural feature	0.009	Removed
Texture_maxcorr	Textural feature	0.000	Removed

The results for validating LULC classification are presented in Table 2. The RF model

demonstrated superior performance, with an average accuracy of 0.843 and an average F1 score of 0.835, as compared to the SVM model, which had an average accuracy of 0.798 and an average F1 score of 0.789. This aligns with findings from previous studies, where RF demonstrated superior performance (Loukika *et al.*, 2021; Talukdar *et al.*, 2020). However, contrasting results have also been reported, with some studies finding SVM more effective under specific conditions (Abdi, 2020). These variations underscore the significant influence of training sample quality, spatial heterogeneity, and regional characteristics on the performance of supervised LULC classification models.

In this study, sample points for training the algorithms were generated through visual inspection, which introduces a potential risk of errors in the training data. However, the RF algorithm's unique structure enables it to be resilient to noisy data by minimizing its influence during training, thereby improving overall classification accuracy (Al-Taei *et al.*, 2023). Also, it is noteworthy that RF exhibited superior performance in adequately fitting the training data (accuracy: 0.995, F1: 0.989). This makes it a highly effective LULC classifier, especially when the training data is diverse, accurate, and plentiful. Based on the above, in keeping with earlier research (Pan *et al.*, 2022; Roy, 2021; Zhong *et al.*, 2021), we observed that the RF algorithm is appropriate for LULC classification via satellite imagery. Thus, it was selected for LULC mapping and further analysis.

Table 2. Validation results of machine learning models. Standard deviation (SD)

Model	Train data				Test data			
	Accuracy		F1		Accuracy		F1	
	Mean	SD	Mean	SD	Mean	SD	Mean	SD
RF	0.995	0.000	0.989	0.001	0.843	0.021	0.835	0.025
SVM	0.915	0.023	0.901	0.022	0.798	0.125	0.789	0.130

3.2. Land use/land cover (LULC) change simulation

3.2.1. Transition suitability maps

Before applying the CA-Markov simulation, to improve the LULC transitions, we reviewed relevant literature and identified key factors influencing these changes. Numerous studies have highlighted that factors such as elevation, slope, distance to roads, and soil type are significant drivers of LULC changes (Geist and Lambin, 2002; Lambin *et al.*, 2001; Veldkamp and Lambin, 2001). The impact of the selected factors on LULC transitions were then quantified by experts. We employed the Analytic Hierarchy Process (AHP) using the Super Decision software and assigned a relative weight to each driver factor. This helped to systematically evaluate the relative importance of factors for each LULC transition, as summarized in Table 3.

Once the driving factors and their respective weights were defined, the next step involved normalizing the factors to ensure comparability. Each factor was normalized to a scale of 0 to 1 using standard normalization techniques, where 0 represented the least suitability and 1 represented the highest suitability for land use/cover transition. Following normalization, the factors were combined using a linear weighted formula. This formula applied the predefined weights to each normalized factor, reflecting their relative importance, and calculated the overall transition suitability value for each point. The resulting transition suitability maps are presented in Figure 3.

Table 3. Key factors influencing LULC transitions and their relative importance weight

Transition to	Influential factor	Explanation	Influence weight
Water	Elevation	Higher areas reduce water buildup and flooding, while lower areas increase it.	0.211
	Slope	Flat areas hold more water, helping form water bodies.	0.421
	Soil Type	Soil type affects water retention and the formation of water bodies.	0.368
Trees	Elevation	Trees grow better at lower elevations due to warmer, moister conditions.	0.261
	Slope	Gentle slopes retain more moisture and have less erosion, which helps trees grow.	0.297
	Soil type	Fertile, well-drained soils are best for tree growth; poor soils limit tree development.	0.342
Wetlands	Elevation	Low-lying areas, which accumulate water, are more likely to become wetlands.	0.284
	Slope	Gentle slopes help water stay in one place, supporting wetland formation.	0.325
	Soil Type	Hydric soils, which hold water, are essential for wetlands and their vegetation.	0.366
Croplands	Distance to roads	Being close to roads helps with transportation of crops, machinery, and supplies.	0.350
	Slope	Flat or gently sloping areas are ideal for farming; steep slopes are harder to farm.	0.400
	Soil type	Fertile soils with good drainage are essential for productive agriculture and crop yields.	0.250
Built-up lands	Distance to roads	Proximity to roads makes urban development easier by improving transportation and access to infrastructure.	0.563
	Slope	Flat or gently sloping areas are easier to develop; steep slopes are harder to urbanize.	0.437
Barren	Elevation	Higher elevations often experience more precipitation.	0.281
	Slope	Steep slopes are prone to erosion, which can lead to barren land.	0.320
	Soil type	Poor soil quality, such as erosion-prone, saline, or compacted soils, leads to barren land.	0.359
Rangeland	Slope	Gentle to moderately steep slopes reduce erosion and help maintain vegetation needed for rangeland.	0.470
	Soil type	Soil quality impacts vegetation health and rangeland productivity.	0.530

We utilized the NASA-DEM digital elevation model (Aeronautics and Laboratory, 2020) with a spatial resolution of 30 m within the Google Earth Engine platform to generate elevation and slope angle maps. The soil texture map, featuring a spatial resolution of 250 m and encompassing twelve classes of the TEB, was derived from the OpenLandMap Soil Texture Class dataset (USDA System) (Hengl, 2018). Additionally, the road layer was sourced from OpenStreetMap on January 3, 2025.

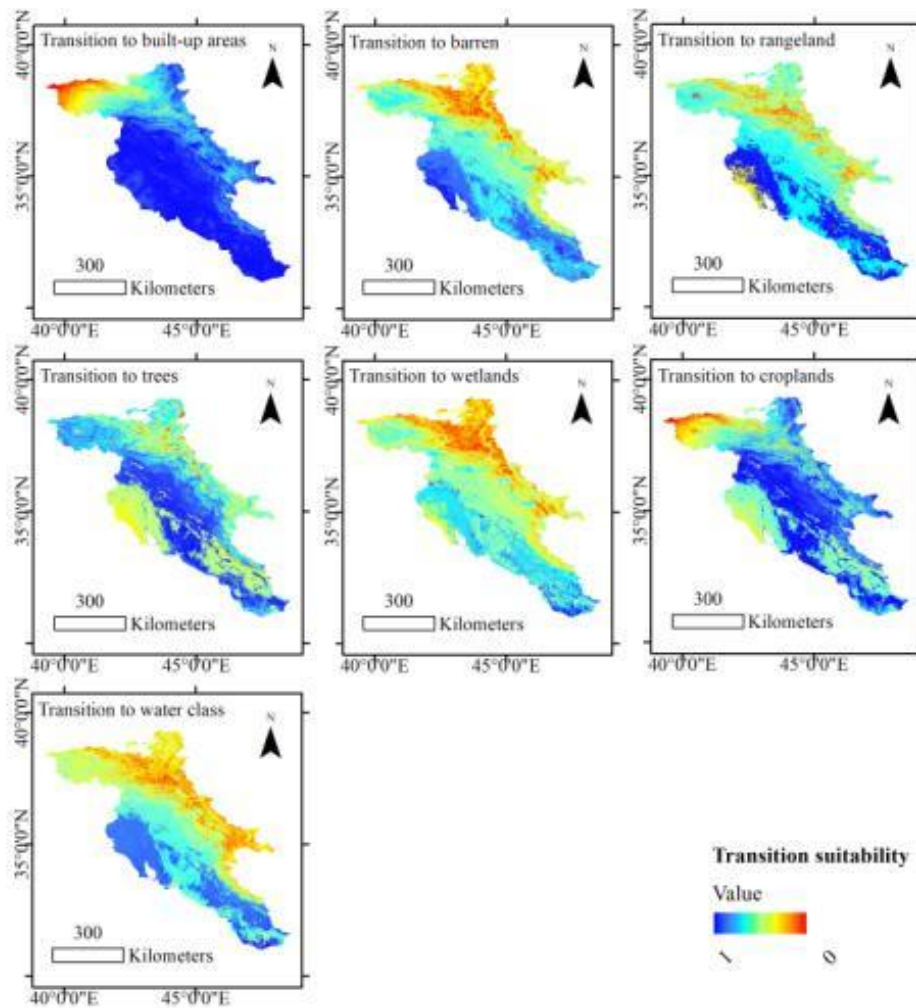


Figure 3. Suitability maps for LULC transition

3.2.2. Transition probabilities

Prior to simulating LULC changes, we enhanced the generalizability of LULC maps by applying the majority filter and boundary clean tools. The majority filter effectively edits individual pixel values that are dissimilar to their surrounding major neighbors whereas boundary clean ensures smoothing of LULC class boundaries.

Following the above-mentioned preprocessing steps, the Markov chain transition matrix was computed by analyzing the LULC changes that transpired during the years 2018 through 2023 (Table 4). Based on the analysis, for water, trees, wetlands, croplands, built-up lands, barren, and rangeland classes, the most probable LULC class in the next state would be water (0.906), trees (0.723), wetlands (0.457), croplands (0.806), built-up lands (0.661), barren (0.828), rangeland (0.897).

According to the findings, the three most unstable LULC classes identified are wetlands, trees, and built-up lands. Wetlands, with the lowest probability of persistence (0.457), are highly vulnerable to hydrological drought and anthropogenic factors such as dam construction, both of which disrupt natural water cycles and contribute to habitat degradation, as observed in the study area over the past years (Al-Taei *et al.*, 2024). Trees, with a moderate instability score (0.723), face threats from deforestation and land-use changes, driven by agricultural expansion and urban

development, consistent with trends highlighted in literature (Al-Taei *et al.*, 2023). Built-up lands (0.661), despite their high stability, may be influenced by misclassification during LULC mapping. This is because built-up areas often exhibit spectral similarities to bare ground, making it challenging to distinguish between these classes, particularly in arid and semi-arid regions with mixed land-use patterns (Rasul *et al.*, 2018).

Table 4. Markov chain transition matrix

Initial state	Probability of next state						
	Water	Trees	Wetlands	Croplands	Built-up lands	Barren	Rangeland
Water	0.906	0	0.005	0.036	0.007	0.035	0.012
Trees	0.001	0.723	0.001	0.033	0	0	0.242
Wetlands	0.093	0.003	0.457	0.377	0.011	0.042	0.016
Croplands	0.005	0	0.001	0.806	0.009	0.028	0.15
Built-up lands	0.011	0	0.001	0.19	0.661	0.047	0.09
Barren	0.001	0	0	0.047	0.002	0.728	0.222
Rangeland	0.001	0.002	0	0.05	0.002	0.049	0.897

3.2.3. Transition simulation

Integrating suitability maps with the Markov transition matrix was crucial for accurately simulating both the quantity and spatial distribution of land use/cover changes. The Markov transition matrix provided transition probabilities between LULC classes, while the suitability maps added spatial context by highlighting areas most suitable for each transition based on driving factors. These combined inputs were fed into the CA spatial filter, which iteratively allocated LULC changes, prioritizing locations with higher suitability values as indicated by the suitability maps.

Accordingly, the CA model was applied to simulate the 2023 and 2028 LULC maps. In this study, longer-term predictions were not pursued to minimize uncertainties and ensure more dependable modeling outcomes. While TRB is undergoing climate-induced changes (Lu *et al.*, 2019), shorter-term predictions using Markov models are more reliable, as their assumptions of stationary transition probabilities are less applicable over extended periods under changing conditions (Chang and Niu, 2023).

Lastly, the 2023 simulated map underwent validation with the one created by classifying Landsat images. Consequently, the proposed approach obtained an average accuracy and F1 of 0.798 and 0.789, correspondingly (Figure 4). The classified and simulated LULC maps are displayed in Figure 5.

Temporal changes in the LULC area were calculated using prepared LULC maps (Table 5). We observed that the tree class has experienced a decline due to urban expansion (Al-Taei *et al.*, 2023), reduced water flows in rivers, and drought (Ozguler and Yildiz 2020). It should be emphasized that the loss of trees may increase the risk of climate change, floods, and soil erosion (Kafy *et al.*, 2021). Wetlands are another area that has experienced decline. The main challenges faced by these areas include controlling the rivers that feed wetlands, managing droughts, and reducing water consumption (Qaderi Nasab and Rahnama, 2020). In recent years, TRB has struggled with water scarcity (Rateb *et al.*, 2021), which has caused certain parts of

the wetlands in this region to dry up.

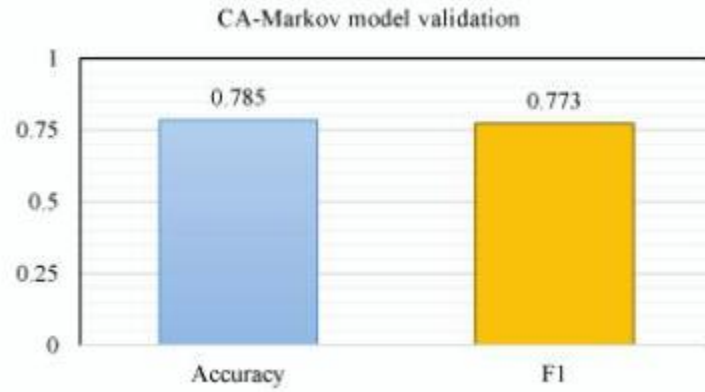


Figure 4. Validation results of CA-Markov model

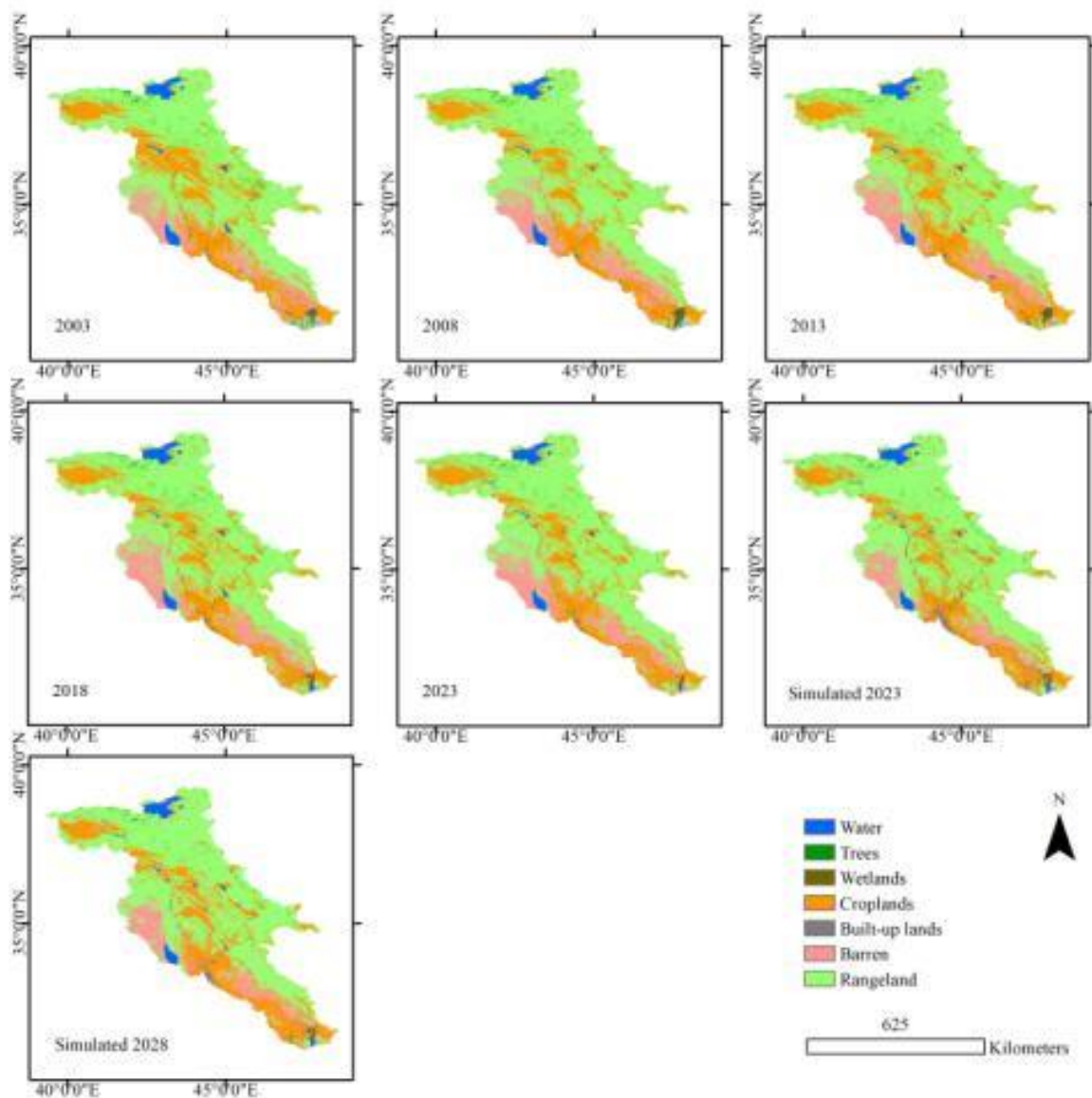


Figure 5. Classified (2003-2023) and simulated (2023 and 2028) LULC maps of the study area

Rangeland areas have diminished along with soil degradation (Bolo *et al.*, 2019), loss of biodiversity (Li *et al.*, 2020), increased erosion risk (Al-Taei *et al.*, 2023), and reduced productivity (Polley *et al.*, 2017) serving as the principal consequences of this concern. Water resources in TRB are also in a perilous state. This study has identified a decline in water resources, which are facing increased stress from dam construction, reduced precipitation, and amplified crop production resulting in augmented water usage (Bolorani *et al.*, 2022; Darvishi Bolorani *et al.*, 2021). Along with social and political issues (Glass, 2017), water shortage can result in environmental deterioration, such as diminished water purity and higher desertification rates.

We also found an expansion of barren areas and built-up lands in TRB. The impact of drought on TRB water resources has decreased availability, causing bare ground to spread. Furthermore, the construction of the Ilisu Dam on the Tigris River in Turkey has reduced water flows, exacerbating water shortages and resulting in the expansion of bare ground in Iraq (Al-Madhhachi *et al.*, 2020). Regarding the expansion of built-up lands, it can be stated that urbanization in TRB lacks a clear strategy and proper urban policy (Al-Taei *et al.*, 2023). Therefore, rapid urban expansion remains one of the leading environmental problems in this region.

In summary, our research provides evidence of the unstable landscape of TRB which may lead to negative consequences, as observed LULC changes are associated with environmental difficulties. Hence, it is essential to implement practical policies and resource management strategies to tackle the situation in TRB effectively.

Table 5. Temporal changes in the area of LULC classes

		2003	2008	2013	2018	2023	Simulated 2028
Water	Area (Km ²)	8163	7076	7552	7441	7315	7248
	Change (%)	-	-13	7	-1	-2	-1
Trees	Area (Km ²)	2785	2319	2190	2119	1926	1803
	Change (%)	-	-17	-6	-3	-9	-6
Wetlands	Area (Km ²)	1757	1883	1588	842	523	344
	Change (%)	-	7	-16	-47	-38	-34
Croplands	Area (Km ²)	72773	62779	69512	66978	64919	63331
	Change (%)	-	-14	11	-4	-3	-2
Built-up lands	Area (Km ²)	1294	1868	2222	2635	2867	3038
	Change (%)	-	44	19	19	9	6
Barren	Area (Km ²)	31878	37026	34938	34640	36032	36858
	Change (%)	-	16	-6	-1	4	2
Rangeland	Area (Km ²)	160485	166187	161137	164483	165558	167010
	Change (%)	-	4	-3	2	1	1

(%)

3.3. Comprehensive discussion

The impact of Ilisu dam in Turkey is evident, in accordance with the aforementioned observations. While we detected the reduction of wetlands, some evidence suggests that the Ilisu dam has also caused a decrease in water levels in the Tigris River, resulting in a decline in the water supply to the Hour al-Azim wetland (Zamani and Berelian, 2022). If the Hour al-Azim wetland dries up, it will become a dust prone source in the region, and dust storm emission will have destructive effects on the surrounding countries. In addition to the above-mentioned consequences of reducing water resources, the Ilisu Dam may also reduce the water quality of the Tigris River and its tributaries and increase the salinity of the Persian Gulf (Zamani and Berelian, 2022). Considering the vast and unique ecosystem of the Tigris River, reducing its water quality can have unpredictable and harmful consequences (Haghighi *et al.*, 2023), leading to endangerment of aquatic life, destruction of agricultural lands, and salinization of a large area of the surrounding lands. Also, increasing salt concentration in the Persian Gulf could have widespread detrimental socio-environmental effects. These effects include threatening the diversity of the Persian Gulf ecosystem, loss of habitat structure, and negative impacts on fishery and tourism. Additionally, community shifts may occur. (Paparella *et al.*, 2022; Röthig *et al.*, 2023).

4. Conclusion

In recent years, climate change and human activities have had various adverse effects on TRB, making the study of its LULC changes is a crucial endeavor. This study examined TRB's LULC changes between 2003 and 2023 through the classification of Landsat images by RF and prediction of the 2028 state using the CA-Markov model. We observed that RF was as a highly practical supervised model for LULC classification, as it was less sensitive to outlier and demonstrated exceptional accuracy in accurately fitting the train data and predicting the new samples. However, the literature suggests that LULC classification models' effectiveness varies across regions, highlighting the significant impact of conditioning spatial factors on supervised algorithms. Additionally, this study found that incorporating morphological features improved the results and is recommended for classifying LULC in large regions with diverse topography.

From an environmental perspective, this study provides evidence of the unstable landscapes of TRB and the resulting adverse impacts in the near future. Our forecast indicates a considerable reduction in vegetation coverage and water resources. These can lead to widespread adverse impacts, including climate change, flooding, increased risk of erosion, drying up of wetlands, loss of biodiversity, soil degradation, reduced productivity and desertification. Meanwhile, the construction of the Ilisu Dam on the Tigris River in Turkey has worsened the situation by exacerbating water shortages, expanding bare ground, harming wetlands, reducing water quality, soil salinization, and damaging the aquatic ecosystem. The drying wetlands and expanding bare grounds will become potential dust sources in the future, and affect surrounding countries. Accordingly, effective policies and resource management practices are essential to address the TRB condition efficiently.

Author contributions

Conceptualization, Abolfazl Ghanbari and Mehrdad Jeihouni; methodology, Abolfazl Ghanbari, Mehrdad Jeihouni, Ayat Khaleel–Gharibawi and Hala Abdulkareem-Rubaiee; software, Ayat Khaleel–Gharibawi and Hala Abdulkareem-Rubaiee; validation, Abolfazl Ghanbari, Ayat Khaleel–Gharibawi and Hala Abdulkareem-Rubaiee; formal analysis, Ayat

Khaleel–Gharibawi and Hala Abdulkareem-Rubaiee; investigation, Abolfazl Ghanbari, Ayat Khaleel–Gharibawi and Hala Abdulkareem-Rubaiee; resources, Ayat Khaleel–Gharibawi and Hala Abdulkareem-Rubaiee; writing—original draft preparation, Ayat Khaleel–Gharibawi and Hala Abdulkareem-Rubaiee; writing—review and editing, Abolfazl Ghanbari and Mehrdad Jeihouni; visualization, Ayat Khaleel–Gharibawi and Hala Abdulkareem-Rubaiee; supervision, Abolfazl Ghanbari; project administration, Abolfazl Ghanbari.

Data Availability Statement

Not applicable.

Acknowledgment

Funding

This research did not receive any specific grant from funding agencies in the public, commercial, or not-for-profit sectors.

Conflict of interest

The authors declare no conflict of interest.

References

- Abatzoglou, J. T., Dobrowski, S. Z., Parks, S. A., & Hegewisch, K. C. (2018). TerraClimate, a high-resolution global dataset of monthly climate and climatic water balance from 1958–2015. *Scientific data*, 5(1), 1-12.
- Abdi, A. M. (2020). Land cover and land use classification performance of machine learning algorithms in a boreal landscape using Sentinel-2 data. *GIScience & Remote Sensing*, 57(1), 1-20.
- Aeronautics, N., & Laboratory, S. A. J. P. (2020). Nasadem merged dem global 1 arc second v001 [data set]. *NASA EOSDIS Land Processes DAAC*.
- Al-Madhhachi, A.-S. T., Rahi, K. A., & Leabi, W. K. (2020). Hydrological impact of ilisu dam on Mosul Dam; the river Tigris. *Geosciences*, 10(4), 120.
- Al-Taei, A. I., Alesheikh, A. A., & Darvishi Bolorani, A. (2023). Land Use/Land Cover Change Analysis Using Multi-Temporal Remote Sensing Data: A Case Study of Tigris and Euphrates Rivers Basin. *Land*, 12(5), 1101.
- Al-Taei, A. I., Alesheikh, A. A., & Darvishi Bolorani, A. (2024). Hazardous Dust Source Susceptibility Mapping in Wet and Dry Periods of the Tigris-Euphrates Basin: A Meta-Heuristics and Machine Learning. *Environmental Management Hazards*, 10(4), 355-370.
- Aryal, J., Sitaula, C., & Frery, A. C. (2023). Land use and land cover (LULC) performance modeling using machine learning algorithms: a case study of the city of Melbourne, Australia. *Scientific reports*, 13(1), 13510.
- Atef, I., Ahmed, W., & Abdel-Maguid, R. H. (2023). Future land use land cover changes in El-Fayoum governorate: a simulation study using satellite data and CA-Markov model. *Stochastic Environmental Research and Risk Assessment*, 1-14.

- Basheer, S., Wang, X., Farooque, A. A., Nawaz, R. A., Liu, K., Adekanmbi, T., & Liu, S. (2022). Comparison of land use land cover classifiers using different satellite imagery and machine learning techniques. *Remote Sensing*, *14*(19), 4978.
- Beroho, M., Briak, H., Cherif, E. K., Boulahfa, I., Ouallali, A., Mrabet, R., Kebede, F., Bernardino, A., & Aboumaria, K. (2023). Future scenarios of land use/land cover (LULC) based on a CA-markov simulation model: case of a mediterranean watershed in Morocco. *Remote Sensing*, *15*(4), 1162.
- Bolo, P. O., Sommer, R., Kihara, J. M., Kinyua, M., Nyawira, S., & Notenbaert, A. M. O. (2019). Rangeland degradation: Causes, consequences, monitoring techniques and remedies. *CIAT Publication*.
- Bolorani, A. D., Najafi, M. S., Soleimani, M., Papi, R., & Torabi, O. (2022). Influence of Hamoun Lakes' dry conditions on dust emission and radiative forcing over Sistan plain, Iran. *Atmospheric Research*, *272*, 106152.
- Brown, C. F., Brumby, S. P., Guzder-Williams, B., Birch, T., Hyde, S. B., Mazzariello, J., Czerwinski, W., Pasquarella, V. J., Haertel, R., & Ilyushchenko, S. (2022). Dynamic World, Near real-time global 10 m land use land cover mapping. *Scientific data*, *9*(1), 251.
- Capolupo, A., Monterisi, C., & Tarantino, E. (2020). Landsat images classification algorithm (LICA) to automatically extract land cover information in Google Earth Engine environment. *Remote Sensing*, *12*(7), 1201.
- Chang, L.-L., & Niu, G.-Y. (2023). The Impacts of Interannual Climate Variability on the Declining Trend in Terrestrial Water Storage over the Tigris–Euphrates River Basin. *Journal of Hydrometeorology*, *24*(3), 549-560.
- Chen, W., Liu, L., Zhang, C., Wang, J., Wang, J., & Pan, Y. (2004). Monitoring the seasonal bare soil areas in Beijing using multitemporal TM images. IGARSS 2004. 2004 IEEE International Geoscience and Remote Sensing Symposium,
- Darvishi Bolorani, A., Papi, R., Soleimani, M., Karami, L., Amiri, F., & Samany, N. N. (2021). Water bodies changes in Tigris and Euphrates basin has impacted dust storms phenomena. *Aeolian Research*, *50*, 100698.
- Diek, S., Fornallaz, F., Schaepman, M. E., & De Jong, R. (2017). Barest pixel composite for agricultural areas using landsat time series. *Remote Sensing*, *9*(12), 1245.
- El Haj, F. A., Ouadif, L., & Akhssas, A. (2023). Simulating and predicting future land-use/land cover trends using CA-Markov and LCM models. *Case Studies in Chemical and Environmental Engineering*, *7*, 100342.
- El Naqa, I., & Murphy, M. J. (2015). *What is machine learning?* Springer.
- Farhangi, F. (2022). Investigating the role of data preprocessing, hyperparameters tuning, and type of machine learning algorithm in the improvement of drowsy EEG signal modeling. *Intelligent Systems with Applications*, *15*, 200100.
- Farhangi, F., Sadegh-Niaraki, A., Vahid Razavi-Termeh, S., & Nahvi, A. (2023). Driver drowsiness modeling based on spatial factors and electroencephalography using machine learning methods: A simulator study. *Transportation Research Part F: Traffic Psychology and Behaviour*, *98*, 123-140. <https://doi.org/https://doi.org/10.1016/j.trf.2023.08.007>

- Farhangi, F., Sadeghi-Niaraki, A., Nahvi, A., & Razavi-Termeh, S. V. (2022). Spatial modelling of accidents risk caused by driver drowsiness with data mining algorithms. *Geocarto International*, 37(9), 2698-2716.
- Farhangi, F., Sadeghi-Niaraki, A., Razavi-Termeh, S. V., & Choi, S.-M. (2021). Evaluation of tree-based machine learning algorithms for accident risk mapping caused by driver lack of alertness at a national scale. *Sustainability*, 13(18), 10239.
- Faruque, M. J., Vekerdy, Z., Hasan, M. Y., Islam, K. Z., Young, B., Ahmed, M. T., Monir, M. U., Shovon, S. M., Kakon, J. F., & Kundu, P. (2022). Monitoring of land use and land cover changes by using remote sensing and GIS techniques at human-induced mangrove forests areas in Bangladesh. *Remote Sensing Applications: Society and Environment*, 25, 100699.
- Feng, Q., Liu, J., & Gong, J. (2015). UAV remote sensing for urban vegetation mapping using random forest and texture analysis. *Remote Sensing*, 7(1), 1074-1094.
- Francini, M., Salvo, C., Viscomi, A., & Vitale, A. (2022). A Deep Learning-Based Method for the Semi-Automatic Identification of Built-Up Areas within Risk Zones Using Aerial Imagery and Multi-Source GIS Data: An Application for Landslide Risk. *Remote Sensing*, 14(17), 4279.
- Geist, H. J., & Lambin, E. F. (2002). Proximate causes and underlying driving forces of tropical deforestation: Tropical forests are disappearing as the result of many pressures, both local and regional, acting in various combinations in different geographical locations. *BioScience*, 52(2), 143-150.
- Gharaibeh, A., Shaamala, A., Obeidat, R., & Al-Kofahi, S. (2020). Improving land-use change modeling by integrating ANN with Cellular Automata-Markov Chain model. *Heliyon*, 6(9).
- Ghayour, L., Neshat, A., Paryani, S., Shahabi, H., Shirzadi, A., Chen, W., Al-Ansari, N., Geertsema, M., Pourmehdi Amiri, M., & Gholamnia, M. (2021). Performance evaluation of sentinel-2 and landsat 8 OLI data for land cover/use classification using a comparison between machine learning algorithms. *Remote Sensing*, 13(7), 1349.
- Giovanis, E., & Ozdamar, O. (2021). The transboundary effects of climate change and global adaptation: The case of the Euphrates-Tigris water basin in Turkey and Iraq. *Available at SSRN 4320746*.
- Glass, S. (2017). Twisting the tap: water scarcity and conflict in the Euphrates-Tigris River basin.
- Haghighi, A. T., Akbari, M., Noori, R., Mehr, A. D., Gohari, A., Sönmez, M. E., Abou Zaki, N., Yilmaz, N., & Kløve, B. (2023). The impact of Turkey's water resources development on the flow regime of the Tigris River in Iraq. *Journal of Hydrology: Regional Studies*, 48, 101454.
- Hengl, T. (2018). Soil texture classes (USDA system) for 6 soil depths (0, 10, 30, 60, 100 and 200 cm) at 250 m (Version v02)[Data set]. Zenodo. In.
- Issa, I. E., Al-Ansari, N., Sherwany, G., & Knutsson, S. (2014). Expected future of water resources within Tigris–Euphrates rivers basin, Iraq. *Journal of Water Resource and Protection*, 6(5), 421-432.

- Jamali, A. (2020). Land use land cover mapping using advanced machine learning classifiers: A case study of Shiraz city, Iran. *Earth Science Informatics*, 13(4), 1015-1030.
- Kafy, A.-A., Al Rakib, A., Akter, K. S., Rahaman, Z. A., Mallik, S., Nasher, N. R., Hossain, M. I., & Ali, M. Y. (2021). Monitoring the effects of vegetation cover losses on land surface temperature dynamics using geospatial approach in Rajshahi City, Bangladesh. *Environmental Challenges*, 4, 100187.
- Kang, J., Fang, L., Li, S., & Wang, X. (2019). Parallel cellular automata Markov model for land use change prediction over MapReduce framework. *ISPRS International Journal of Geo-Information*, 8(10), 454.
- Khorrami, M., Khorrami, M., & Farhangi, F. (2022). Evaluation of tree-based ensemble algorithms for predicting the big five personality traits based on social media photos: Evidence from an Iranian sample. *Personality and Individual Differences*, 188, 111479. <https://doi.org/10.1016/j.paid.2021.111479>
- Lambin, E. F., Turner, B. L., Geist, H. J., Agbola, S. B., Angelsen, A., Bruce, J. W., Coomes, O. T., Dirzo, R., Fischer, G., & Folke, C. (2001). The causes of land-use and land-cover change: moving beyond the myths. *Global environmental change*, 11(4), 261-269.
- Li, W., Buitenwerf, R., Chequín, R. N., Florentín, J. E., Salas, R. M., Mata, J. C., Wang, L., Niu, Z., & Svenning, J.-C. (2020). Complex causes and consequences of rangeland greening in South America—multiple interacting natural and anthropogenic drivers and simultaneous ecosystem degradation and recovery trends. *Geography and Sustainability*, 1(4), 304-316.
- Loukika, K. N., Keesara, V. R., & Sridhar, V. (2021). Analysis of land use and land cover using machine learning algorithms on google earth engine for Munneru River Basin, India. *Sustainability*, 13(24), 13758.
- Lu, Y., Wu, P., Ma, X., & Li, X. (2019). Detection and prediction of land use/land cover change using spatiotemporal data fusion and the Cellular Automata–Markov model. *Environmental monitoring and assessment*, 191, 1-19.
- Mishra, V. N., Prasad, R., Rai, P. K., Vishwakarma, A. K., & Arora, A. (2019). Performance evaluation of textural features in improving land use/land cover classification accuracy of heterogeneous landscape using multi-sensor remote sensing data. *Earth Science Informatics*, 12, 71-86.
- Mohanaiah, P., Sathyanarayana, P., & GuruKumar, L. (2013). Image texture feature extraction using GLCM approach. *International journal of scientific and research publications*, 3(5), 1-5.
- Momeni, R., Aplin, P., & Boyd, D. S. (2016). Mapping complex urban land cover from spaceborne imagery: The influence of spatial resolution, spectral band set and classification approach. *Remote Sensing*, 8(2), 88.
- Mondal, M. S., Sharma, N., Garg, P. K., & Kappas, M. (2016). Statistical independence test and validation of CA Markov land use land cover (LULC) prediction results. *The Egyptian Journal of Remote Sensing and Space Science*, 19(2), 259-272.
- Ozguler, H., & Yildiz, D. (2020). Consequences of the droughts in the Euphrates-Tigris Basin. *International Journal of Water Management and Diplomacy*, 1(1), 29-40.

- Pan, X., Wang, Z., Gao, Y., Dang, X., & Han, Y. (2021). Detailed and automated classification of land use/land cover using machine learning algorithms in Google Earth Engine. *Geocarto International*, 1-18.
- Pan, X., Wang, Z., Gao, Y., Dang, X., & Han, Y. (2022). Detailed and automated classification of land use/land cover using machine learning algorithms in Google Earth Engine. *Geocarto International*, 37(18), 5415-5432.
- Paparella, F., D'Agostino, D., & A. Burt, J. (2022). Long-term, basin-scale salinity impacts from desalination in the Arabian/Persian Gulf. *Scientific reports*, 12(1), 20549.
- Polley, H. W., Bailey, D. W., Nowak, R. S., & Stafford-Smith, M. (2017). Ecological consequences of climate change on rangelands. *Rangeland systems: Processes, management and challenges*, 229-260.
- Qaderi Nasab, F., & Rahnama, M. (2020). Developing restoration strategies in Jazmurian wetland by remote sensing. *International Journal of Environmental Science and Technology*, 17, 2767-2782.
- Rasul, A., Balzter, H., Ibrahim, G. R. F., Hameed, H. M., Wheeler, J., Adamu, B., Ibrahim, S. a., & Najmaddin, P. M. (2018). Applying built-up and bare-soil indices from Landsat 8 to cities in dry climates. *Land*, 7(3), 81.
- Rateb, A., Scanlon, B. R., & Kuo, C.-Y. (2021). Multi-decadal assessment of water budget and hydrological extremes in the Tigris-Euphrates Basin using satellites, modeling, and in-situ data. *Science of The Total Environment*, 766, 144337.
- Röthig, T., Trevathan-Tackett, S. M., Voolstra, C. R., Ross, C., Chaffron, S., Durack, P. J., Warmuth, L. M., & Sweet, M. (2023). Human-induced salinity changes impact marine organisms and ecosystems. *Global Change Biology*, 29(17), 4731-4749.
- Roy, B. (2021). A machine learning approach to monitoring and forecasting spatio-temporal dynamics of land cover in Cox's Bazar district, Bangladesh from 2001 to 2019. *Environmental Challenges*, 5, 100237.
- Roy, P. S., Ramachandran, R. M., Paul, O., Thakur, P. K., Ravan, S., Behera, M. D., Sarangi, C., & Kanawade, V. P. (2022). Anthropogenic land use and land cover changes—A review on its environmental consequences and climate change. *Journal of the Indian Society of Remote Sensing*, 50(8), 1615-1640.
- Siddiqui, A., Siddiqui, A., Maithani, S., Jha, A. K., Kumar, P., & Srivastav, S. K. (2018). Urban growth dynamics of an Indian metropolitan using CA Markov and Logistic Regression. *The Egyptian Journal of Remote Sensing and Space Science*, 21(3), 229-236.
- Singh, G., & Pandey, A. (2021a). Evaluation of classification algorithms for land use land cover mapping in the snow-fed Alaknanda River Basin of the Northwest Himalayan Region. *Applied Geomatics*, 13(4), 863-875.
- Singh, G., & Pandey, A. (2021b). Evaluation of classification algorithms for land use land cover mapping in the snow-fed Alaknanda River Basin of the Northwest Himalayan Region. *Applied Geomatics*, 13, 863-875.

- Singh, R. P., Singh, N., Singh, S., & Mukherjee, S. (2016). Normalized difference vegetation index (NDVI) based classification to assess the change in land use/land cover (LULC) in Lower Assam, India. *International Journal of Advanced Remote Sensing and GIS*, 5(10), 1963-1970.
- Talukdar, S., Singha, P., Mahato, S., Pal, S., Liou, Y.-A., & Rahman, A. (2020). Land-use land-cover classification by machine learning classifiers for satellite observations—A review. *Remote Sensing*, 12(7), 1135.
- Tassi, A., Gigante, D., Modica, G., Di Martino, L., & Vizzari, M. (2021). Pixel-vs. Object-based landsat 8 data classification in google earth engine using random forest: The case study of maiella national park. *Remote Sensing*, 13(12), 2299.
- Veldkamp, A., & Lambin, E. F. (2001). Predicting land-use change. In (Vol. 85, pp. 1-6): Elsevier.
- Wang, J., Bretz, M., Dewan, M. A. A., & Delavar, M. A. (2022). Machine learning in modelling land-use and land cover-change (LULCC): Current status, challenges and prospects. *Science of The Total Environment*, 822, 153559.
- Xu, H. (2006). Modification of normalised difference water index (NDWI) to enhance open water features in remotely sensed imagery. *International journal of remote sensing*, 27(14), 3025-3033.
- Yeneneh, N., Elias, E., & Feyisa, G. L. (2022). Detection of land use/land cover and land surface temperature change in the Suha Watershed, North-Western highlands of Ethiopia. *Environmental Challenges*, 7, 100523.
- Zamani, S. G., & Berelian, P. (2022). Construction and operation of Ilisu Dam by the Turkish government in the context of international law. *Public Law Studies Quarterly*, 1-27.
- Zhong, B., Yang, A., Jue, K., & Wu, J. (2021). Long Time Series High-Quality and High-Consistency Land Cover Mapping Based on Machine Learning Method at Heihe River Basin. *Remote Sensing*, 13(8), 1596.
- Zucca, C., Middleton, N., Kang, U., & Liniger, H. (2021). Shrinking water bodies as hotspots of sand and dust storms: The role of land degradation and sustainable soil and water management. *Catena*, 207, 105669.